CERN-TH.3987/84
ERRATUM

DRELL-YAN CROSS SECTIONS AT SMALL TRANSVERSE MOMENTUM

C.T.H.Davies, B.R. Webber
Cavendish Laboratory, Univ. of Cambridge
Cambridge CB3 OHE, U.K.

and

W.J. Stirling
CERN - Geneva

ERRATA

(i) On page 6, Eq. (10) should read

$$\begin{aligned} P(x) = {} & C_F^2 \left[-2\,\frac{1+x^2}{1-x}\ln x \ln(1-x) - \left(2+4x+\frac{3}{1-x}\right)\ln x \right. \\ & \left. -\tfrac{1}{2}(1+x)\ln^2 x - 9(1-x) + 2\,\frac{1+x^2}{1+x}\,S(x) \right] \\ & + C_F C_A \left[\frac{1+x^2}{1-x}\left(\tfrac{1}{2}\ln^2 x + \frac{11}{6}\ln x + \frac{67}{18} - \frac{\pi^2}{6}\right) \right. \\ & \left. + 2(1+x)\ln x + \tfrac{26}{3}(1-x) - \frac{1+x^2}{1+x}\,S(x) \right] \\ & + C_F T_R \left[\frac{1+x^2}{1-x}\left(-\tfrac{2}{3}\ln x - \tfrac{10}{9}\right) - \tfrac{4}{3}(1-x) \right] \end{aligned}$$

(ii) Appendix 2 should be relabelled Table I and should also include

$$C_N^{(1)} = C_F\left(\frac{\pi^2}{2} - 4 + \frac{1}{(N+1)(N+2)}\right)$$

CERN-TH.3987/84
August 1984
ERRATUM

CERN-TH.3987/84

DRELL-YAN CROSS SECTIONS AT SMALL TRANSVERSE MOMENTUM

C.T.H.Davies, B.R. Webber
Cavendish Laboratory, Univ. of Cambridge
Cambridge CB3 OHE, U.K.

and

W.J. Stirling
CERN - Geneva

ABSTRACT

We present QCD predictions for the production of vector bosons at small transverse momentum in hadron-hadron collisions by the Drell-Yan mechanism. By using Fermilab and ISR data to fix the parametrization of non-perturbative effects we are able to define clearly the region of transverse momentum in which a leading logarithm analysis applies for the production of W and Z bosons. We also investigate the sensitivity of the cross-section to recently calculated coefficients in this analysis.

CERN-TH.3987/84
August 1984

1. Introduction

The transverse momentum (q_T) distribution of lepton pairs produced by the Drell-Yan process is of considerable theoretical interest as it should provide a good test of QCD. In the naive parton model the only source of transverse momentum is an intrinsic component associated with the motion of quarks inside hadrons, with $\langle q_T^2 \rangle \sim 1$ (GeV/c)^2. In QCD the quarks which annihilate to form the vector boson can pick up transverse momentum by gluon radiation, producing a much broader distribution.

A difficulty in calculating the q_T spectrum in QCD is that there are collinear and soft singularities associated with the emission of real gluons. These are cancelled by diagrams containing virtual gluons (except for those collinear singularities which are to be associated with the structure functions), but the cancellation is not complete when $q_T^2 \ll Q^2$ (= dilepton-mass-squared) since the virtual gluon phase space is not inhibited by a condition on q_T whereas the real gluon phase space is. The result is that large logarithms $\ell n(Q^2/q_T^2)$ appear multiplying α_s, so that a perturbative calculation to fixed order in α_s is not sensible. Since most of the cross-section is at small q_T it is important to find a way of summing these large logarithms to all orders.

Much progress has been made since the early work of Dokshitzer, D'yakonov and Troyan[1], but the structure of the result remains the same. The Fourier-Bessel transform of the cross-section factorizes into two structure functions (D) and a form factor (T) which contains the large logarithms from the soft and collinear gluon emission.

In a previous paper[2] the coefficients of some of the logarithms

in T were calculated from the $O(\alpha_s^2)$ differential cross-section $s\frac{d\sigma}{dt\ du}$ for the production of a virtual photon. In section 2 we briefly review the results obtained there and report a value for the previously undetermined coefficient $B^{(2)}$.

In sections 3 and 4 we describe the numerical calculation of the cross-section using these coefficients and compare the results with experiment. Data from Fermilab and the ISR serve mainly to fix non-perturbative parameters which dominate at low Q^2. The production of W and Z bosons at the CERN $p\bar{p}$ collider, on the other hand, provides an excellent opportunity for testing the form factor T, since we now have values of Q^2 such that there is genuinely a region of q_T in which $\Lambda^2 << q_T^2 << Q^2$, where the large logarithms $\ell n(Q^2/q_T^2)$ will dominate other terms. Using the parameters from the lower-Q^2 data we can clearly define this region and show the relative importance of the different calculated coefficients there.

2. Calculation of the form factor

The general result for the small-q_T cross-section for $A+B\to\gamma^* X\to\ell^+\ell^- X$ to all orders in α_s is of the form [3),4)]

$$\frac{Q^2}{\sigma_o}\frac{d^2\sigma}{dQ^2 dq_T^2} = \int dx_A dx_B\ \delta(x_A x_B - \frac{Q^2}{s})\ \frac{1}{2}\int_o^\infty db\ b\ J_o(bq_T) e^{-S(b,Q)}$$
$$\times \sum_f e_f^2 \{ D_{q_f/A}(x_A, {}^{b_o}/_b)\ D_{\bar{q}_f/B}(x_B, {}^{b_o}/_b) + \{q \leftrightarrow \bar{q}\}\} \qquad (1)$$

$$\sigma_o = \frac{4\pi\alpha^2}{9s}$$

$$b_o = 2\ e^{-\gamma_E}$$

All corrections which vanish in the limit $q_T \to 0$ are ignored in equation (1). The function $D_{q/A}$ is the quark structure function for quark q in hadron A and e^{-S} is the Sudakov-like form factor, called T in section 1.

The coefficients A and B are defined by writing

$$S(b,Q) = \int_{(b_{o/b})^2}^{Q^2} \frac{dq^2}{q^2} \left\{ \ln \frac{Q^2}{q^2} \; A(\alpha_s(q)) + B(\alpha_s(q)) \right\}$$

$$A(\alpha_s) = \sum_{i=1}^{\infty} \left(\frac{\alpha_s}{2\pi} \right)^i A^{(i)} \qquad (2)$$

$$B(\alpha_s) = \sum_{i=1}^{\infty} \left(\frac{\alpha_s}{2\pi} \right)^i B^{(i)}$$

A and B may of course be changed by redefining the limits of the integral in (2) and keeping the value of S(b,Q) the same[3]. We believe that A and B have the simplest expressions using the limits above.

As in Ref. 2 our derivation of the coefficients is done using the quantity Σ,

$$\Sigma = \int_0^1 d\tau \; \tau^N \; \frac{Q^2}{\sigma_o} \; \frac{d^2\sigma}{dQ^2 dq_T^2} \; , \qquad \tau = \frac{Q^2}{s} \qquad (3)$$

$$= \sum_f e_f^2 \; \frac{1}{2} \int_0^{\infty} db \; b \; J_o(bq_T) \; e^{-S(b,Q)}$$

$$\times \left\{ D_{q_{f/A}}(N, {}^{b_{o/b}}) \; D_{\bar{q}_{f/B}}(N, {}^{b_{o/b}}) + q \leftrightarrow \bar{q} \right\}$$

where the Nth moments with respect to τ are taken at fixed Q^2, integrating over s. In this section we specialize to the non-singlet case so that D refers to the valence quark distribution $q_f - \bar{q}_f$. The nth moments of these distributions can be written

$$D_{NS}(N, {}^{b_o}/_{b}) = d(N, {}^{b_o}/_{b}, \alpha_s(\mu), \mu)\ f_{q/A}\ (N,\mu) \qquad (4)$$

where f represents the probability distribution for a valence quark in a hadron A at renormalisation scale μ [i.e. we take the factorisation mass M equal to the renormalisation point μ]. d satisfies the usual renormalisation group equation, whose solution is

$$d = C_N\ (\alpha_s({}^{b_o}/_{b}))\ \exp\{ - \int_{({}^{b_o}/_{b})^2}^{\mu^2} \frac{dq^2}{q^2}\ \gamma_N(\alpha_s(q))\}$$

$$C_N = 1 + \sum\ (\frac{\alpha_s}{2\pi})^i\ C_N^{(i)} \qquad (5)$$

$$\gamma_N = \sum\ (\frac{\alpha_s}{2\pi})^i\ \gamma_N^{(i)}$$

where $\gamma_N^{(i)}$ are the anomalous dimensions for the space-like evolution of the non-singlet quark density $(q_f - \bar{q}_f)$.

If we write the quantity Σ as

$$\Sigma = \sum_f e_f^2\ [f_{q/A}\ (N,\mu)\ f_{\bar{q}/B}(N,\mu) + q \leftrightarrow \bar{q}] \qquad (6)$$

$$\times \frac{1}{2} \int_0^\infty db\ b\ J_0(bq_T)\ \exp[\ \sum_{n=1}^{\infty}\ \sum_{m=0}^{n+1}\ (\frac{\alpha_s}{2\pi})^n\ (\ell n\ \frac{Q^2 b^2}{b_o^2})^m\ {}_nD_m(N,t)\ ]$$

$$\alpha_s \equiv \alpha_s(\mu)$$

then the ${}_nD_m$ can be written in terms of $A^{(i)}$, $B^{(i)}$, $C_N^{(i)}$, $\gamma_N^{(i)}$ and $t = \ell n\ \frac{Q^2}{\mu^2}$. By expanding the exponential and taking the Bessel transform we can write

$$\Sigma = \sum_f e_f^2 \left[f_{q/A}(N,\mu)\, f_{\bar{q}/B}(N,\mu) + q \leftrightarrow \bar{q} \right]$$
$$\times \left\{ \sum_{n=1}^{\infty} \sum_{m=o}^{2n-1} \left(\frac{\alpha_s}{2\pi}\right)^n \left(\ell n \frac{Q^2}{q_T^2}\right)^m {}_nC_m(N,t) \right\} \qquad (7)$$

where the ${}_nC_m$ are expressible in terms of the ${}_nD_m$. By comparing this expression with a calculation of Σ at $O(\alpha_s^n)$ we can find values for ${}_nC_m$ and therefore for $A^{(i)}$, $B^{(i)}$ and $C_N^{(i)}$.

As in Ref. 2 we use the work of Ellis, Martinelli and Petronzio[5] who have calculated at $O(\alpha_s^2)$ the parton level cross-section $s\frac{d\sigma}{dtdu}$. By analytic integration over kinematic variables at fixed Q^2, q_T^2 in the limit $q_T \to 0$ we derive a form for the parton level version of Σ. This is to be compared with equation (7) where $f_{q/A}$ has been replaced by the quark distribution $f_{q/q}$,

$$f_{q/q}(N,\mu) = 1 + \frac{\alpha_s}{2\pi}\gamma_N^{(1)} \left\{ \frac{1}{\varepsilon} + \gamma_E - \ell n\,(4\pi) \right\} \quad , \qquad (8)$$

since the calculation is done using dimensional regularisation and $\overline{MS}$ renormalisation.

In Ref. 2 we discussed the results from a calculation of ${}_1C_1$, ${}_1C_0$, ${}_2C_3$, ${}_2C_2$ and ${}_2C_1$ which confirmed the structure of equation (6) and gave values for the coefficients $A^{(2)}$ and $C_N^{(1)}$ (see Table 1). Equation (6) predicts that ${}_2C_0$ should have the form[2]

$${}_2C_0 = B^{(2)} + 2\gamma_N^{(2)} + C_F^2 \left[8\zeta(3) - 3\pi^2 + 24 \right.$$
$$\left. - \frac{6}{(N+1)(N+2)} + \xi_N \left(2\pi^2 - 16 + \frac{4}{(N+1)(N+2)} - 6t\right) + 4\xi_N^2\, t \right] \qquad (9)$$
$$- C_F \left(\frac{11}{6} C_A - \frac{2}{3} T_R\right) \left(\pi^2 - 8 + \frac{2}{(N+1)(N+2)} - 3t + 2t\,\xi_N\right)$$

where $C_F\,\xi_N = \gamma_N^{(1)}$

We find

$$\gamma_N^{(2)} = \int_0^1 dx\, x^N \,[P(x)]_+ \tag{10}$$

where

$$\begin{aligned} P(x) = C_F^2\Big[&-2\,\frac{1+x^2}{1-x}\,\ell n\, x\,\ell n(1-x) - \Big(2 + 4x + \frac{3}{1-x}\Big)\,\ell n\, x \\ &- \frac{1}{2}\,(1+x)\,\ell n^2 x - 9(1-x) - 2\,\frac{1+x^2}{1+x}\,S(x)\Big] \\ &+ C_F C_A\Big[\,\frac{1+x^2}{1-x}\,\Big(\frac{1}{2}\,\ell n^2 x + \frac{11}{6}\,\ell n x + \frac{67}{18} - \frac{\pi^2}{6}\Big) \\ &\qquad + \frac{14}{3}\,(1-x) + \frac{1+x^2}{1+x}\,S(x)\Big] \\ &+ C_F T_R\Big[\,\frac{1+x^2}{1-x}\,\Big(-\frac{2}{3}\,\ell n x - \frac{10}{9}\Big) - \frac{4}{3}\,(1-x)\Big] \end{aligned}$$

and $S(x) = -\frac{1}{2}\,\ell n^2 x + 2\ell n x\,\ell n(1+x) + 2Li_2(-x) + \frac{\pi^2}{6}$, which is identical to the second-order space like non-singlet $(q_f - \bar{q}_f)$ kernel determined by Curci et al [6].

We also find

$$\begin{aligned} B^{(2)} = &\; C_F^2\Big\{\pi^2 - \frac{3}{4} - 12\,\zeta(3)\Big] \\ &+ C_F C_A\Big[\,\frac{11}{9}\,\pi^2 - \frac{193}{12} + 6\zeta(3)\Big] \\ &+ C_F T_R\Big[-\frac{4}{9}\,\pi^2 + \frac{17}{3}\Big] \end{aligned} \tag{11}$$

The form of the $A^{(i)}$ and $B^{(i)}$ is rather interesting. Kodaira and Trentadue[4] have argued that the leading contribution to the cross-

section as $q_T \to 0$ is determined by the behaviour of the non-singlet Altarelli-Parisi functions. Thus $A^{(1)}$ should be the coefficient of the leading $(1-x)^{-1}$ singularity in the lowest order kernel $P_{qq}^{(1)}(x)$, and $B^{(1)}$ is twice the integral over the non-singular remainder. Kodaira and Trentadue worked in a light-like axial gauge, in which the term proportional to $A^{(1)}$ arises from the emission of soft and collinear gluons by the quark line when the gauge vector is along the antiquark line. The term with coefficient $B^{(1)}$ is due to emission of gluons, at least one of which is not soft, from both lines and also from interference terms between emissions from each line. (Using a different gauge would give the same values for $A^{(1)}$ and $B^{(1)}$ but they would be produced from different diagrams.)

Kodaira and Trentadue further conjectured that $A^{(2)}$ would arise in a similar way to $A^{(1)}$ from the second order space like non-singlet Altarelli-Parisi kernel for $(q_f - \bar{q}_f)\ P_{qq}^{(2)}(x)$. This was confirmed by the results of Ref. 2. We now find that $B^{(2)}$ differs from twice the integral over the non-singular parts of $P^{(2)}(x)$ only by a term proportional to β_0. The origin of this extra term is unclear but it does appear that not all logarithms at $O(\alpha_s^2)$ can be derived from the Altarelli-Parisi kernel and there is a contribution from gluons which are soft but not collinear. For reference, we collect in Table 1 the expressions for all the coefficients we have calculated and their numerical values.

3. Calculation of the cross-section

We now describe how equation (1) may be used to compute values for the cross-section $d\sigma/dq_T^2$ for virtual photon production at small transverse momentum. $e^{-S(b,Q)}$ is flavour independent so the same $A^{(i)}$ and $B^{(i)}$ coefficients arise in the general cross-section as those presented in section 2 for the non-singlet case. In that section we expanded S in terms of $\alpha_s(\mu)$ to compare with an $O(\alpha_s^2)$ calculation. We can now use a form for S which includes the terms in all orders that are generated from $A^{(i)}$ and $B^{(i)}$ by the running of the coupling constant (at 2 loop order).

This gives a form factor $e^{-S(b,Q)}$ which strongly suppresses the large b region. It is shown in Fig.1 together with the effect of successively adding the coefficients $B^{(1)}$, $A^{(2)}$ and $B^{(2)}$ to $A^{(1)}$. It is encouraging to note that the contributions of successive terms are decreasing. The shape of the form factor depends chiefly on the value of ℓnQ. For larger Q values it falls much more sharply with increasing b.

The structure functions in equation (1) become more complicated when the singlet contribution is included as we must consider gluon initiated processes. The structure functions defined by equation (1) are not the same as those measured in deep inelastic scattering (DIS) which are defined by

$$\frac{F_2(x,k)}{x} = \sum_f e_f^2 \left[D'_{q_{f/A}}(x,k) + D'_{\bar{q}_{f/A}}(x,k) \right] \qquad (12)$$

The relationship $D_{q_{f/A}} = D'_{q_{f/A}}$ is spoiled by the different finite $O(\alpha_s)$ corrections to the two processes.

We find, writing

$$Q'(x_A,x_B,k) = D'_{q/A}(x_A,k)\, D'_{\bar{q}/B}(x_B,k) + (q\leftrightarrow\bar{q})$$

$$G'_A(x_A,x_B,k) = [D'_{q/B} + D'_{\bar{q}/B}]\, D'_{g/A} \qquad (13)$$

$$G'_B(x_A,x_B,k) = [D'_{q/A} + D'_{\bar{q}/B}]\, D'_{g/B}$$

that, to this order

$$\begin{aligned} Q(x_A,x_B,{}^{b_o}/_b) &= Q'(x_A,x_B,{}^{b_o}/_b) \\ &+ \frac{\alpha_s({}^{b_o}/_b)}{2\pi} C_F\Big[\int_{x_A}^1 \frac{dz}{z} f_q(z)\, Q'(\frac{x_A}{z}, x_B, {}^{b_o}/_b) \\ &\qquad + \int_{x_B}^1 \frac{dz}{z} f_q(z)\, Q'(x_A,\frac{x_B}{z}, {}^{b_o}/_b)\Big] \\ &+ \frac{\alpha_s({}^{b_o}/_b)}{2\pi}\, \frac{1}{2}\, \Big[\int_{x_A}^1 \frac{dz}{z} f_g(z)\, G'_A(\frac{x_A}{z}, x_B, {}^{b_o}/_b) \\ &\qquad + \int_{x_B}^1 \frac{dz}{z} f_g(z)\, G'_B(x_A,\frac{x_B}{z}, {}^{b_o}/_b)\Big] \end{aligned} \qquad (14)$$

where

$$\begin{aligned} f_q(z) &= \frac{3}{2}\, \frac{1}{(1-z)_+} - (1+z^2)\Big[\frac{\ell n(1-z)}{1-z}\Big]_+ + \Big[\frac{1+z^2}{1-z}\Big]\ell n\, z \\ &\quad - 2 - 3z + (\frac{1}{2} + \frac{5\pi^2}{6})\,\delta(1-z) \end{aligned} \qquad (15)$$

$$f_g(z) = 1 - 6z(1-z) - [z^2 + (1-z)^2]\,\ell n\,(\frac{1-z}{z})$$

The functions $f_q(z)$ and $f_g(z)$ are the difference between the coefficient functions for structure functions defined in equations (1)

and (12). That the scale of α_s in equation (14) is ${}^{b}o/_{b}$ is shown by the analysis of the coefficient ${}_2C_0$ in section 2, where a term $\beta_o C_N$ [1] is clearly seen. It is generated by expressing $\alpha_s({}^{b}o/_{b})$ in terms of $\alpha_s(\mu)$, the expansion parameter for the ${}_nC_m$. We can define a K factor, K_{DYQT} in a similar way to that for the total DY cross-section, K_{DY} by

$$Q(x_A,x_B,{}^{b}o/_{b}) = K_{DYQT}\ (x_A,x_B,{}^{b}o/_{b})\ Q'(x_A,x_B,{}^{b}o/_{b}) \qquad (16)$$

A study of K_{DY} [7] has shown it to be fairly constant independently of τ, the scale at which the structure functions are evaluated (in this case Q^2) and the type of beam and target hadrons. This is because K_{DY} is dominated, for most values of τ, by the terms proportional to $\delta(1-z)$ that appear in the equivalent of $f_q(z)$.

K_{DYQT} has quite different behaviour. The $\delta(1-z)$ terms in $f_q(z)$ (equation (15)) almost cancel against the other terms so the final contribution comes mainly from the gluon corrections which are sensitive to the type of annihilating hadrons, at least at large τ. The pp and $p\bar{p}$ values of K_{DYQT} are similar at small τ but for large τ the pp K factor becomes much larger [8] (at small scales) because the gluon structure function is harder than the sea. K_{DYQT} is also very scale dependent largely because the corrections appear with $\alpha_s({}^{b}o/_{b})$.

For the DIS structure functions used to calculate $Q'(x_A,x_B,{}^{b}o/_{b})$ in equation (16) we take the recent parametrisation of Duke and Owens,[9] who provide 2 acceptable sets of structure functions, set 1 with

Λ = 0.2 GeV and set 2 with a much harder gluon distribution and Λ = 0.4 GeV. Although their parameter Λ actually corresponds to a lowest order evolution equation, we may take it to represent $\Lambda_{\overline{MS}}$ within the present margin of experimental uncertainty. We shall present results for both sets of structure functions and consider the difference between the cross-sections that arises to be an indication of the uncertainty associated with our poor knowledge of the value of $\Lambda_{\overline{MS}}$.

The Duke and Owens structure functions are parameterised in terms of $s = \ell n \left(\frac{\ell n Q^2/\Lambda^2}{\ell n Q_0^2/\Lambda^2}\right)$ where Q_0 is the starting point for their evolution. They take Q_0 to be 2 GeV, above the charm threshold, so that their evolution equations are consistent with 4 flavours. The structure functions are unreliable below 2 GeV for this reason and also because no target mass corrections or other higher twist effects have been included.

Using these DIS structure functions we are able to calculate values for our K factor K_{DYQT}. The problem is, as usual, that K_{DYQT} is not small, being $\sim$ 1.6 at small scales. We therefore cannot be confident that uncalculated higher order corrections will be negligible.

In the next section we describe the fit to data at low Q^2. Because large b is not very well suppressed at these values of Q^2 the K factor at small scales appears as an overall normalisation to the cross-section, and we might hope, by comparing to the data, that the size of higher order corrections to K_{DYQT} could be assessed. The data, however, have a normalisation uncertainty of $\sim$ 25%.

We find that, for Duke and Owens set 2 structure functions, the predicted cross-section fits the data adequately with only $O(\alpha_s)$ terms

in K_{DYQT}, but for set 1 structure functions it is slightly low. An improved fit is obtained by rewriting the terms explicitly proportional to $\delta(1-z)$ in equation (14) as

$$Q'(x_A, x_B, {}^{b_0}/_{b}) \left[C_F \frac{\alpha_s}{2\pi} \left(1 + \frac{2\pi^2}{3}\right) + \exp\left(\frac{\alpha_s}{2\pi} C_F \pi^2\right) \right] \qquad (16)$$

ie. we perform an exponentiation of 'continuation π'[10] terms which are also found to improve the fit to data of K_{DY}[7].

Figure 2 shows the K factors K_{DYQT} for set 1 and set 2 as a function of $\ell n\ b$ at two values of τ and $y = \frac{1}{2} \ell n\ {}^{x_A}/_{x_B} = 0$. We see that exponentiating the π^2 terms for set 1 and using only $O(\alpha_s)$ terms for set 2 makes the two K factors become very similar at large τ (corresponding to the low energy data) but at small τ (relevant to W and Z production at the collider) the K factor for set 1 is larger (it would be almost the same as that for the set 2 if only $O(\alpha_s)$ terms were considered).

We will use the two different forms of K_{DYQT} consistently throughout section 4, since we want to know the range over which the cross-section can lie within theoretical uncertainties. Altering the set 1 K_{DYQT} by exponentiating π^2 terms produces an effect on the cross-section in the same direction as decreasing Λ so in this way we can combine the two sources of uncertainty.

The integration in equation (1) is from b = 0 to ∞. The summation of large logarithms in b space that we use is only a good approximation for $1/Q < b < 1/\Lambda$. The region of integration between 0 and 1/Q is not a problem because it is suppressed by the kinematic factor b and consequently the way in which we choose to continue the form factor

from $1/Q$ to 0 makes no difference for $q_T < Q/5$. (We take $q_T = Q/5$ to represent the upper limit for our analysis since $O(1)$ is then still large compared to power suppressed terms $O(q_T/Q)$).

The region $b \gtrsim 1/\Lambda$ is more of a problem. The perturbative expansion of S is not reliable in this region and also the structure functions are not defined for scales less than $Q_0 = 2$ GeV. We take Q_0 to represent the lowest scale where perturbation theory is sensible and assume that below this value some non-perturbative effects take over that we can only parameterise.

Following Collins and Soper[11] we define

$$b^* = \frac{b}{\left[1+b^2Q_0^2\right]^{1/2}} \tag{17}$$

so that as $b \to \infty$, $b^* \to 1/Q_0$. In principle we could introduce $Q_1 > Q_0$ in place of Q_0 but this would cause us to lose predictive power since we would then be describing calculable effects by a parameterisation. We rewrite the form factor and structure functions in equation 1 replacing b by b^*; they are thus never evaluated outside the perturbative regime.

The smearing in transverse momentum introduced by non-perturbative effects is taken to be of the form

$$e^{-b^2\left[g_1 + g_2 \ln Q/2Q_0\right]} \tag{18}$$

where we expect $4g_1 = O(Q_0^2)$ since g_1 represents the presence of an intrinsic transverse momentum. The g_2 term reflects the smearing from our failure to resolve gluons with $q_T < Q_0$ as the structure functions evolve from scales $O(Q_0)$ to those $O(Q)$.

So, finally, the equation that we use to calculate the cross-section at small transverse momentum is

$$\frac{Q^2}{\sigma_o}\frac{d\sigma}{dQ^2 dq_T^2 dy} = \frac{1}{2}\int_o^\infty db\, J_o(b\, q_T)\, e^{-S(b^*,Q)}\, e^{-b^2[g_1+g_2 \ell n\, Q/2Q_o]} \times \sum_f e_f^2\, Q(x_A, x_B, {}^{b_o}/_{b^*})$$

$$x_A = \sqrt{\tau} e^{y} \quad X_B = \sqrt{\tau} e^{-y} \qquad (19)$$

replacing equation (1). The only free parameters are g_1 and g_2 which are fixed by comparison with data in Section 4.

4. A Comparison with data

To use equation (19) to calculate the cross-section we need $Q > 7$ GeV, say, to have a reasonable range of q_T for which our analysis is valid. We use data from two experiments: E288 at Fermilab[12] and R209 at the CERN ISR[13], neglecting the region $9 < Q < 11$ GeV which has a considerable contribution from decays of the Υ family.

A study of the form factor at $Q \sim 10$ GeV shows that it is still quite broad in b space (Fig.1). Values of $b \sim 1/Q_o$ are not effectively suppressed and so in b^* space the form factor is almost a constant. The cross-section, therefore, sees no details of the perturbative effects and depends mainly on the smearing factor. This does make the data useful however for finding the values of g_1 and g_2.

Figures 3 and 4 show predicted cross-sections using $g_1 = 0.15$ $(GeV)^2$, $g_2 = 0.4$ $(GeV)^2$ compared to the data from E288 for set 1 and set 2 structure functions respectively. For set 2 structure functions the cross-section for $Q > 11$ GeV is unacceptably far above the data. This

we expect because Duke and Owens[9], in deriving set 2, rejected data on the total DY cross-section from proton-heavy nucleus scattering, on the grounds that the recently noticed 'EMC effect'[14] might indicate that heavy nucleus structure functions were softer than those of individual nucleons. Thus set 2 is allowed a harder gluon distribution than set 1.

It may be that we could still fit the data for $Q > 11$ GeV by introducing a τ dependence into g_1, which is not excluded in principle[11]. (g_2 on the other hand should be independent of τ.) Since we are interested in $\tau < 0.04$ for W and Z cross-sections at the collider, however, we shall ignore the high Q^2 Fermilab data as far as set 2 structure functions are concerned.

Figure 5 shows the predicted cross-section for set 1 and set 2 using the same parameters as before, compared to R209 data. The agreement is well within the errors.

We can now use the values of g_1 and g_2 above to calculate the transverse momentum cross-section for W and Z production at the CERN $p\bar{p}$ collider. The normalisation σ_0/Q^2 in equation (19) must be changed to $\frac{\sqrt{2}\pi G_F}{3}\left(\frac{M_W^2}{s}\right)$ for W production and $\frac{\sqrt{2}\pi G_F}{12}\left(\frac{M_Z^2}{s}\right)$ for Z. We take M_W = 83 GeV, M_Z = 94 GeV. The structure function sums that contribute to $Q(x_A, x_B, {}^{b_o}/_{b})$ become the relevant ones to make W and Z bosons and e_f^2 is changed to the appropriate weak charge[15]. The functions $f_q(z)$ and $f_g(z)$, of course, remain the same. We find that K_{DYQT} has similar behaviour to that shown in Fig. 2 for $\tau = 0.02$.

To compare the predicted distribution of events with data from the collider we need to include the branching fraction for decay of W or Z into the detected decay mode,

$$B(W\to e\nu) = 0.089 \ , \quad B(Z\to e^+e^-) = 0.032 \ , \tag{20}$$

the integrated luminosity received by the detector and the detector efficiency.

Figure 6 gives a comparison of our prediction with the $W\to e\nu$ events from UA1[16]. We use an integrated luminosity 136 nb^{-1} and the quoted UA1 overall efficiency of 0.65 (assumed uniform over the rapidity and p_T of the W, when summing W^+ and W^- events).

A comparison to UA2 results [17] is shown in Fig.7, where we take an integrated luminosity 131 nb^{-1} and detector acceptance 0.5.

The predicted cross-section looks generally narrower than the data but this may be an artefact of the experimental resolution smearing the observed distribution.

It is important to be clear about which regions of the cross-section are a prediction of QCD and which are still dependent on the parameterisation of non-perturbative effects. In Fig.8 we show the effect of changing the smearing function on the cross-section in the 'UA1 units' of Fig. 6. $e^{-0.8b^2}$ and $e^{-1.8b^2}$ are extreme cases requiring values of g_1 and g_2 which are just about compatible with low Q^2 data. [$g_1 = 0.15$ and $g_2 = 0.4$ give $e^{-1.36b^2}$ at the W mass]. We conclude that for $6<q_T<16$ GeV the cross-section receives little contribution from the non-perturbative region of b ($b \gtrsim 1/Q_0$) and so should be a firm prediction of QCD.

For the benefit of future collider experiments we give in Fig.10

the absolute cross-section $d\sigma/dq_T$, integrated over y for the summed production of W^+ and W^- at $\sqrt{s}$ = 630 GeV. The two predictions for set 1 and set 2 structure functions represent the difference between Λ = 0.2 GeV and Λ = 0.4 and include uncertainties from higher order corrections to K_{DYQT} as explained in Section 3. For Λ = 0.4 GeV the cross-section is broader, corresponding to a narrower form factor in b space.

The question to ask now is, how sensitive is the cross-section to the perturbative coefficients that we have calculated? In Fig. 10 we show the effect on the cross-section calculated using set 2 structure functions of successively adding to $A^{(1)}$ the coefficients $B^{(1)}$, $A^{(2)}$ and $B^{(2)}$. We see, as expected from Fig.1 that the size of the contribution to the cross-section decreases in the order $A^{(1)}>B^{(1)}>A^{(2)}>B^{(2)}$. The effect of $A^{(2)}$ is to broaden the cross-section in q_T space by slightly more than the effect of changing Λ from 0.2 GeV to 0.4 GeV (compare Fig.9). $B^{(2)}$, on the other hand, produces very little effect and the unknown next term $A^{(3)}$ probably even less. Roughly speaking $A^{(3)}$ would have to be of the order of 50 for its effect to be comparable with that of $B^{(2)}$.

Turning now to Z° production, Fig. 11 shows the absolute cross-section $d\sigma/dq_T$ at $\sqrt{s}$ = 630 GeV. Its shape is very similar to that for W as ℓnQ has not changed significantly. A comparison with existing collider data is not meaningful as the number of events is so low.

Finally, in Figs. 12 and 13 we give the expected production cross-section $d\sigma/dq_T$ for $(W^+ + W^-)$ and Z° at $\sqrt{s}$ = 2 TeV. The cross-sections are slightly broader than at $\sqrt{s}$ = 540 GeV because τ has now decreased to the point where the structure function sum Q' is increasing with

increasing scale. This behaviour is cancelled by the fall of K_{DYQT} so that $Q(x_A,x_B,{}^{b}o/_{b})$ is almost constant in b space and no longer suppresses the small b region. The peak in the cross-section in q_T space is broadened as a result.

5. Conclusions

We have presented a calculation of the cross-sections for vector boson production at small transverse momentum by the Drell-Yan process. This calculation is based on the summation of large logarithms in b space, whose coefficients we have determined in full to $O(\alpha_s^2)$. Several of these coefficients were previously unknown and we are able to assess their contribution.

Our calculation has the following desirable features:

(1) No terms in the cross-section such as the form factor or structure functions are evaluated outside the perturbative regime. Non-perturbative effects are included in a consistent way via a parameterisation that fits low Q^2 data.

(2) The correct structure functions are included, related to those measured in DIS by a calculated b dependent K factor.

We predict the cross-section for $q_T \lesssim Q/5$. For q_T larger than this our calculation will not be correct since it does not predict the power-suppressed terms which start to dominate there. A recent paper by Altarelli et al[18] successfully joins the full $O(\alpha_s)$ cross-section at high q_T to the all orders leading logarithm result at small q_T. Our treatment of the small q_T region differs mainly in that we have been able to establish that the effect of the extra coefficient $B^{(2)}$ is

fortunately small and that we have, we believe, a more complete treatment of non-perturbative effects based on the approach of Ref. 11) and on a detailed study of lower energy data.

Our main conclusion is then that W and Z production in the region $6<q_T<16$ GeV is insensitive to non-perturbative effects and should be firmly predicted by QCD. The main uncertainty in this region is the value of Λ and we give two sets of predictions, for Λ = 0.2 GeV and Λ = 0.4 GeV.

Appendix 2

The expression for the calculated coefficients and their numerical values.

$$A^{(1)} = 2C_F$$

$$= 2.67$$

$$B^{(1)} = -3C_F$$

$$= -4.0$$

$$A^{(2)} = 2C_F \left[\left(\frac{67}{18} - \frac{\pi^2}{6}\right) C_A - \frac{10}{9} T_R \right]$$

$$= 10.69 - 1.48 \ (N_f - 4)$$

$$B^{(2)} = C_F^2 \left[\pi^2 - \frac{3}{4} - 12 \ \zeta \ (3) \right]$$

$$+ C_F C_A \left[\frac{11}{9} \pi^2 - \frac{193}{12} + 6 \ \zeta \ (3) \right]$$

$$+ C_F T_R \left[- \frac{4}{9} \pi^2 + \frac{17}{3} \right]$$

$$= 6.75 + .85 \ (N_f - 4)$$

References

1) Yu.L. Dokshitzer, D.I. D'yakonov and S.I.Troyan. Phys. Rep. 58 (1980) 269.
For more recent work see references 3)-15) of Ref. 2.

2) C.T.H. Davies and W.J. Stirling, CERN preprint TH.3853 (1984), to appear in Nucl. Phys. B244 (1984) 337.

3) J.C. Collins and D.E. Soper. Nucl. Phys. B193 (1981) 381; B194 (1982) 445; B197 (1982) 446.

4) J. Kodaira and L. Trentadue. Phys. Lett. 112B (1982) 66; 123B (1983) 335.

5) R.K. Ellis, G. Martinelli and R. Petronzio. Phys. Lett. 104B (1981) 45; Nucl. Phys. B211 (1983) 106.

6) G. Curci, W. Furmanski and R. Petronzio. Nucl.Phys. B175 (1980)27.

7) F. Khalafi and W.J. Stirling. Z. Phys. C18 (1983) 315.

8) C.T.H. Davies, Ph.D. Thesis, University of Cambridge (1984).

9) D.W. Duke and J.F. Owens. Phys. Rev. D30 (1984) 49.

10) W.J. Stirling, Proceedings of the Drell-Yan Workshop, Fermilab (1982), 131.

11) J.C. Collins and D.E. Soper, Nucl. Phys. B197 (1982) 446;
J.C. Collins, D.E. Soper and G. Sterman, Proceedings of the Drell-Yan Workshop, Fermilab (1982), 279;
J.C. Collins, D.E. Soper and G. Sterman, CERN preprint TH.3923 (1984).

12) A.S. Ito et al., Phys. Rev. D23 (1981) 604

13) D. Antreasyan et al., Phys. Rev. Lett. 47 (1981) 12; 48 (1982) 302.

14) J.J. Aubert et al., Phys. Lett. 123B (1983) 275.

15) E. Rademacher, CERN preprint EP/84-41 (1984), to be published in Progress in Particle and Nuclear Physics.

16) G. Arnison et al., Phys. Lett. 129B (1983) 273; 134B (1984) 469.

17) P. Bagnaia et al., CERN preprint CERN-EP/84-39, submitted to Z. Phys. (1984).

18) G. Altarelli, R.K. Ellis, M. Greco and G. Martinelli, CERN preprint TH 3851 (1984).

Figure Captions

Fig.1 The form factor $e^{-S(b,Q)}$ as a function of b (in $(GeV)^{-1}$) for Q = 10 GeV, Λ = 0.2 GeV. The solid line shows the form factor with only coefficient $A^{(1)}$, the dashed line has $B^{(1)}$ added, the dot-dashed line includes also $A^{(2)}$ and the dotted line has all calculated coefficients. The unknown coefficient $A^{(3)}$ would need a value greater than 20 for its contribution to be distinguishable from the dotted line.

Fig.2 The K factor K_{DYQT} in b space, for pp scattering at y = 0. The solid line and dashed line use set 2 structure functions, Λ = 0.4 GeV, for τ = 0.16 and 0.02 respectively. Only $O(\alpha_s)$ terms are included in K_{DYQT}. The dot-dashed (τ = 0.16) and dotted lines (τ = 0.02) are for set 1 with Λ = 0.2 GeV and π^2 terms exponentiated in K_{DYQT}. When integrated over y the K factor takes very similar values.

Fig.3 $E\frac{d^3\sigma}{dp^3}$ at y = 0.03 for $\sqrt{s}$ = 27.4 GeV in units of pb $(GeV/c)^{-2}$ for pN scattering where N = 0.4p + 0.6n. The curves are for set 1 structure functions, Λ = 0.2 GeV and non-perturbative smearing as described in the text. The data are from experiment E288 for the following mass bins:

(1) 7<Q<8 GeV

(2) 8<Q<9 GeV

(3) 11<Q<12 GeV

(4) 12<Q<13 GeV

(5) 13<Q<14 GeV

Fig.4 As Fig. 3 except that the curves are for set 2 structure functions, Λ = 0.4 GeV.

Fig.5 $d\sigma/dq_T^2$ integrated over y at $\sqrt{s}$ = 62 GeV, in units of pb $(GeV/c)^{-2}$ for pp scattering. The solid line is for set 1 structure functions, Λ = 0.2 GeV and the dashed line for set 2. The data are from experiment R209 for $11<Q<25$ GeV.

Fig.6 The cross-section for W production at $\sqrt{s}$ = 540 GeV in units of events per 2 GeV/c seen in a detector of efficiency 0.65 after an integrated luminosity 136 nb^{-1}. The dashed line is the set 1 prediction and the dotted line set 2. The data are from the UA1 43 $W\to e\nu$ events.

Fig.7 The cross-section for W production at $\sqrt{s}$ = 540 GeV. Events per 3 GeV/c seen in a detector of efficiency 0.5 after an integrated luminosity of 131 nb^{-1}. Dashed line : set 1, dotted line: set 2. Data are from UA2 37 $W\to e\nu$ events.

Fig.8 Cross-section as for Fig.6 with various smearing factors.
Solid line: $e^{-1.36b^2}$ $[g_1 = 0.15(GeV)^2, g_2 = 0.4(GeV)^2]$
Dashed line: $e^{-0.8b^2}$
Dotted line: $e^{-1.8b^2}$

Fig.9 $d\sigma/dq_T$ in nb $(GeV/c)^{-1}$ for W production at $\sqrt{s}$ = 630 GeV from $p\bar{p}$
Solid line: set 1, Λ = 0.2 GeV
Dashed line: set 2, Λ = 0.4 GeV.

Fig.10 $d\sigma/dq_T$ in $nb(GeV/c)^{-1}$ for W production at $\sqrt{s}$ = 630 GeV, Λ = 0.4 GeV, in $p\bar{p}$ showing the effect of successively adding the calculated coefficients to $e^{-S(b,Q)}$
Dashed-dotted line: $A^{(1)}$ only
Dashed line: add $B^{(1)}$
Dotted line: add $A^{(2)}$
Solid line: add $B^{(2)}$ i.e. the complete $O(\alpha_s^2)$ S(b,Q).

Fig.11 $d\sigma/dq_T$ in $nb(GeV/c)^{-1}$ for Z° production in $p\bar{p}$ at $\sqrt{s}$ = 630 GeV

Solid line: set 1, Λ = 0.2 GeV

Dashed line: set 2, Λ = 0.4 GeV

Fig.12 $d\sigma/dq_T$ for W production at $\sqrt{s}$ = 2 TeV, $p\bar{p}$ in $nb(GeV/c)^{-1}$.

Solid line: set 1, Λ = 0.2 GeV

Dashed line: set 2, Λ = 0.4 GeV.

Fig.13 $d\sigma/dq_T$ for Z° production at $\sqrt{s}$ = 2 TeV, $p\bar{p}$ in $nb(GeV/c)^{-1}$.

Solid line: set 1, Λ = 0.2 GeV

Dashed line: set 2, Λ = 0.4 GeV.

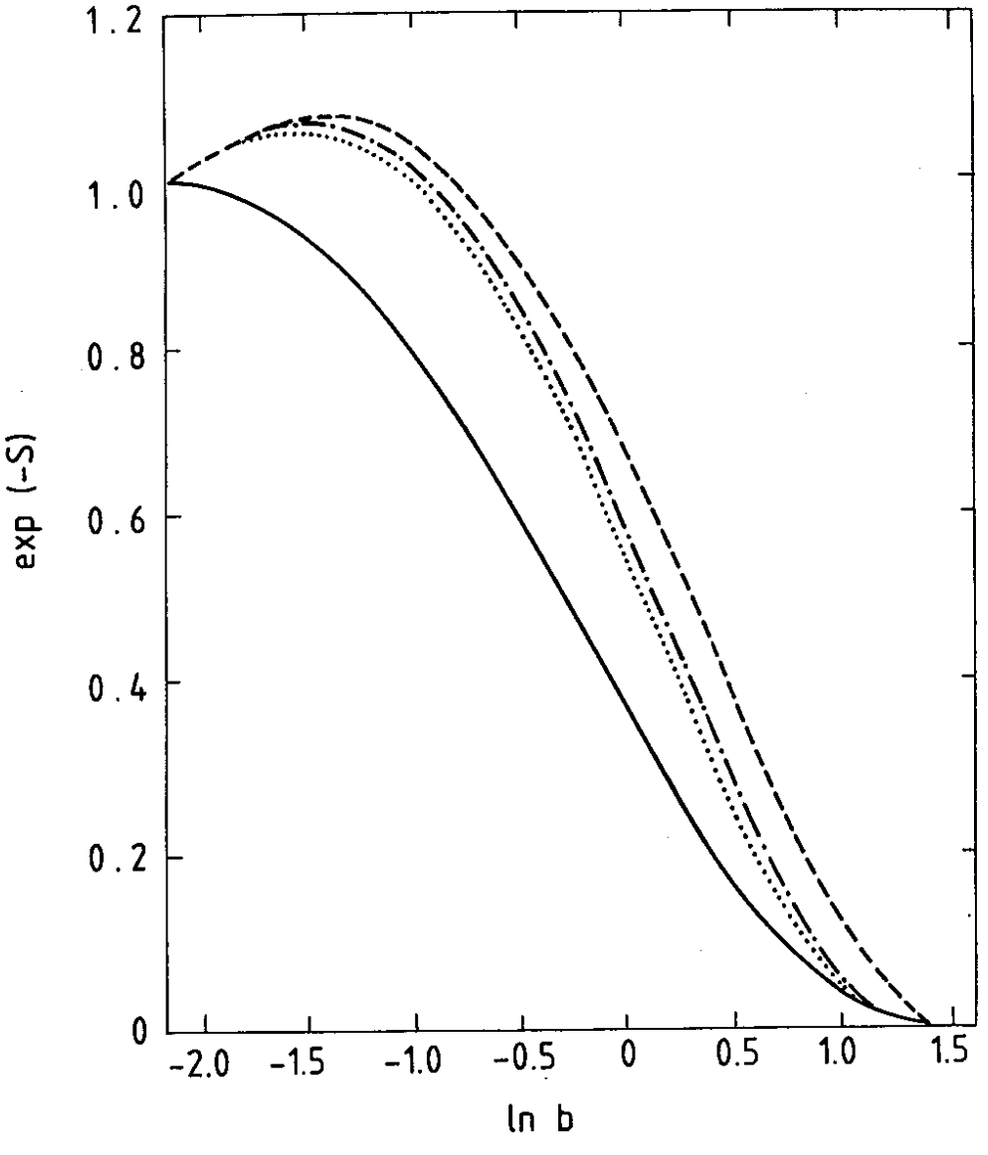
1.2
1.0
0.8
0.6
0.4
0.2
0
exp (-S)
-2.0
-1.5
-1.0
-0.5
0
0.5
1.0
1.5
ln b

Fig. 1

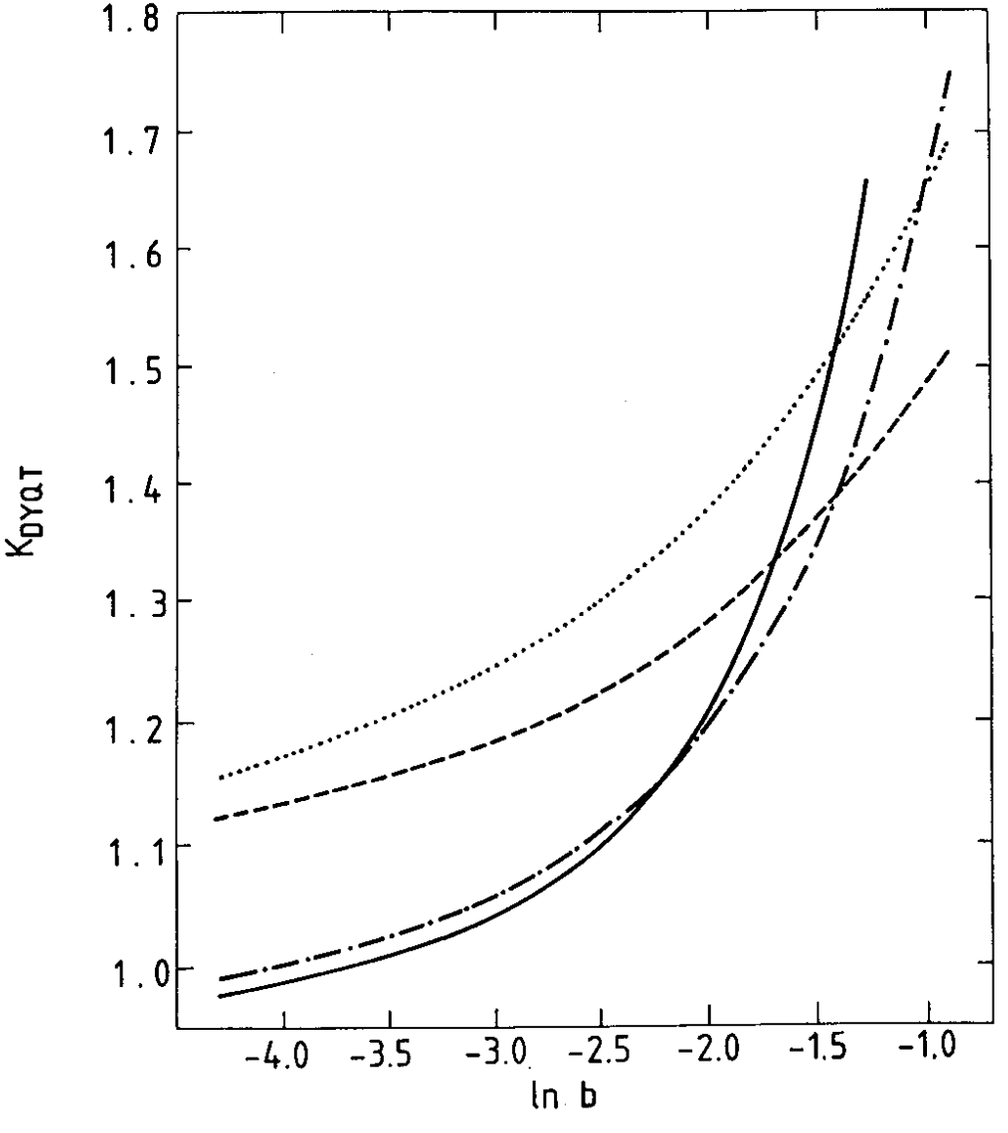
1.8
1.7
1.6
1.5
1.4
1.3
1.2
1.1
1.0
K_DYQT
-4.0
-3.5
-3.0
-2.5
-2.0
-1.5
-1.0
ln b

Fig. 2

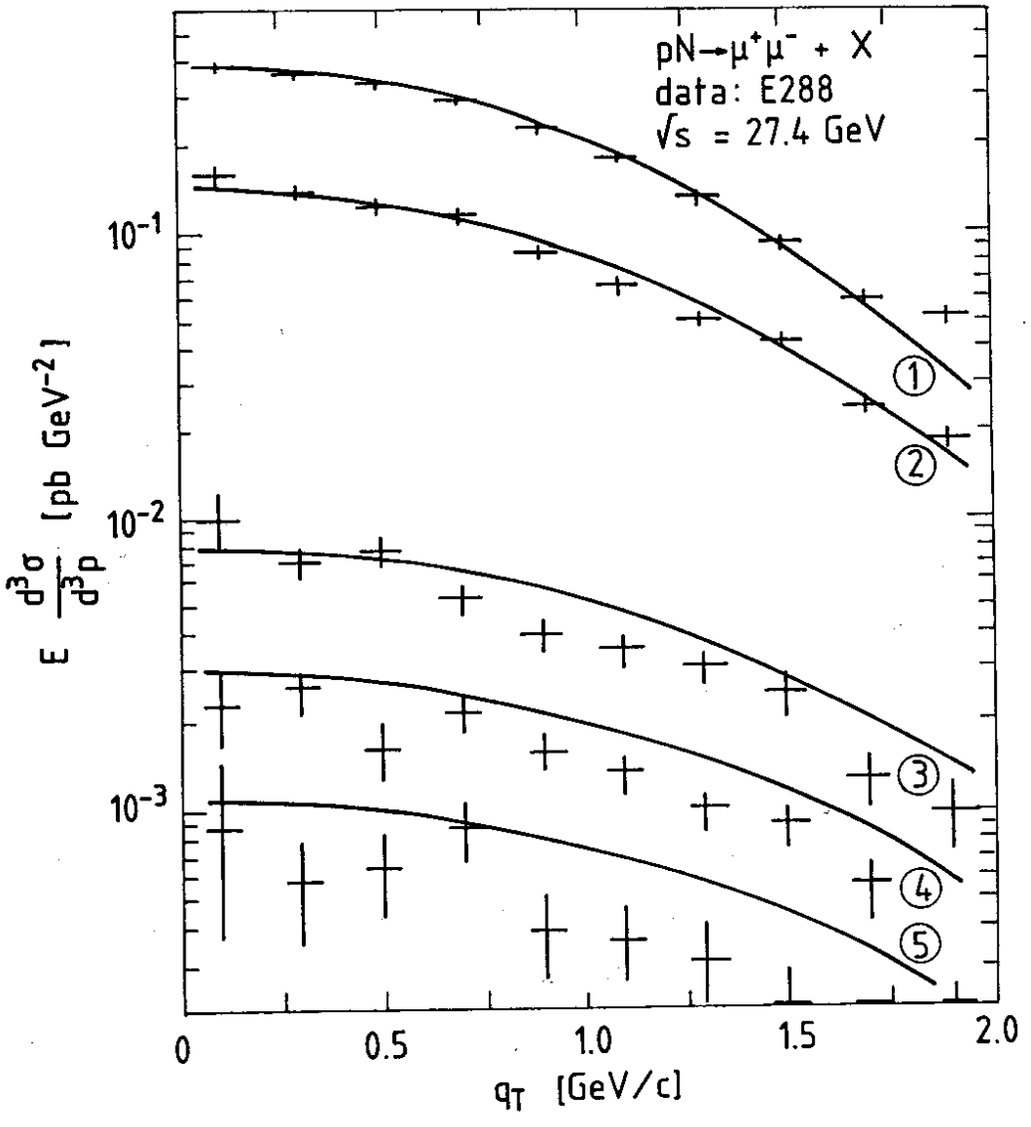
pN→μ⁺μ⁻ + X
data: E288
√s = 27.4 GeV
$E\frac{d^3\sigma}{d^3p}$ [pb GeV^{-2}]
10^{-1}
10^{-2}
10^{-3}
①
②
③
④
⑤
0
0.5
1.0
1.5
2.0
q_T [GeV/c]

Fig. 3

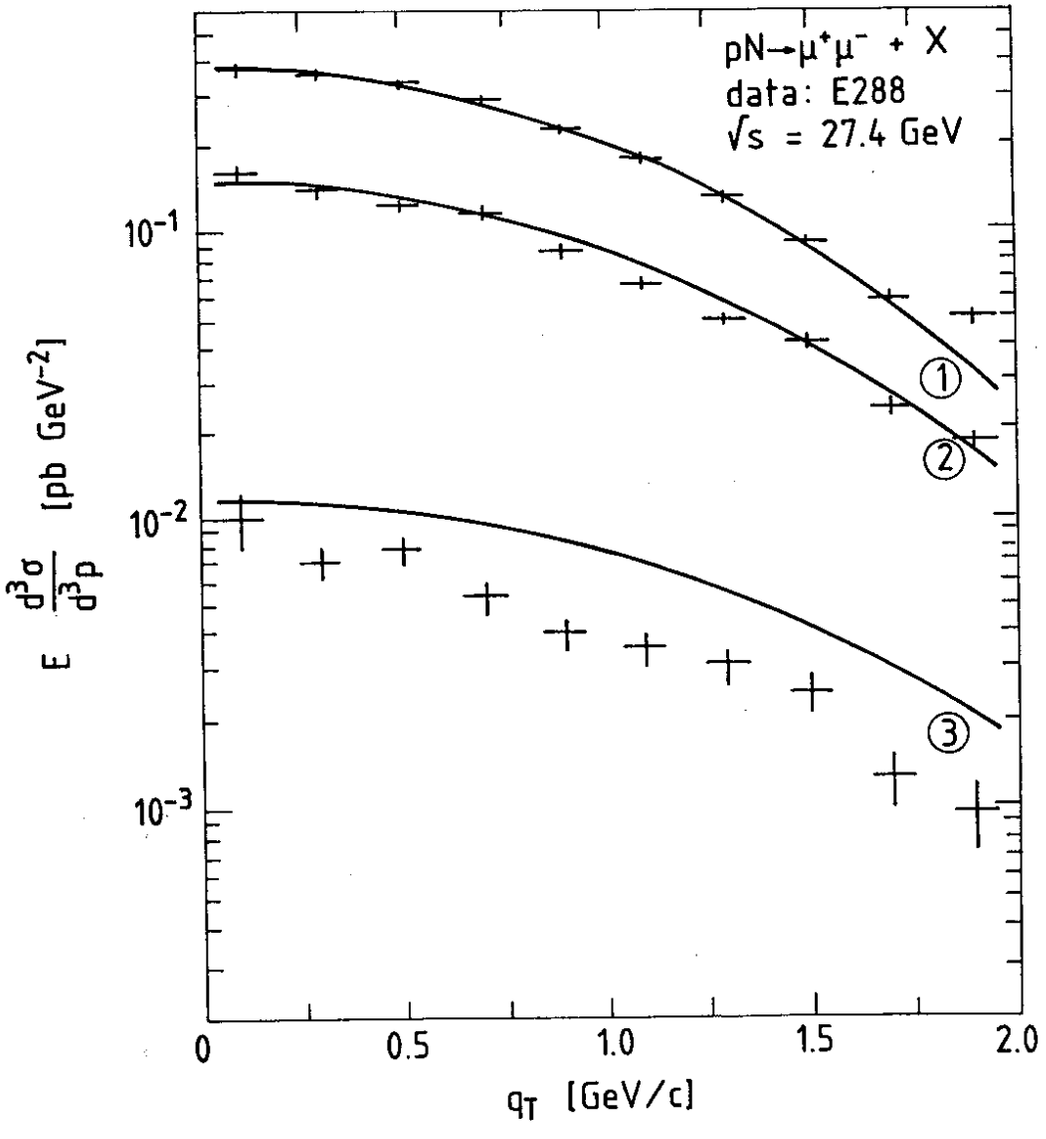
pN→μ⁺μ⁻ + X
data: E288
√s = 27.4 GeV
$E\frac{d^3\sigma}{d^3p}$ [pb GeV^{-2}]
10^{-1}
10^{-2}
10^{-3}
①
②
③
0
0.5
1.0
1.5
2.0
q_T [GeV/c]

Fig. 4

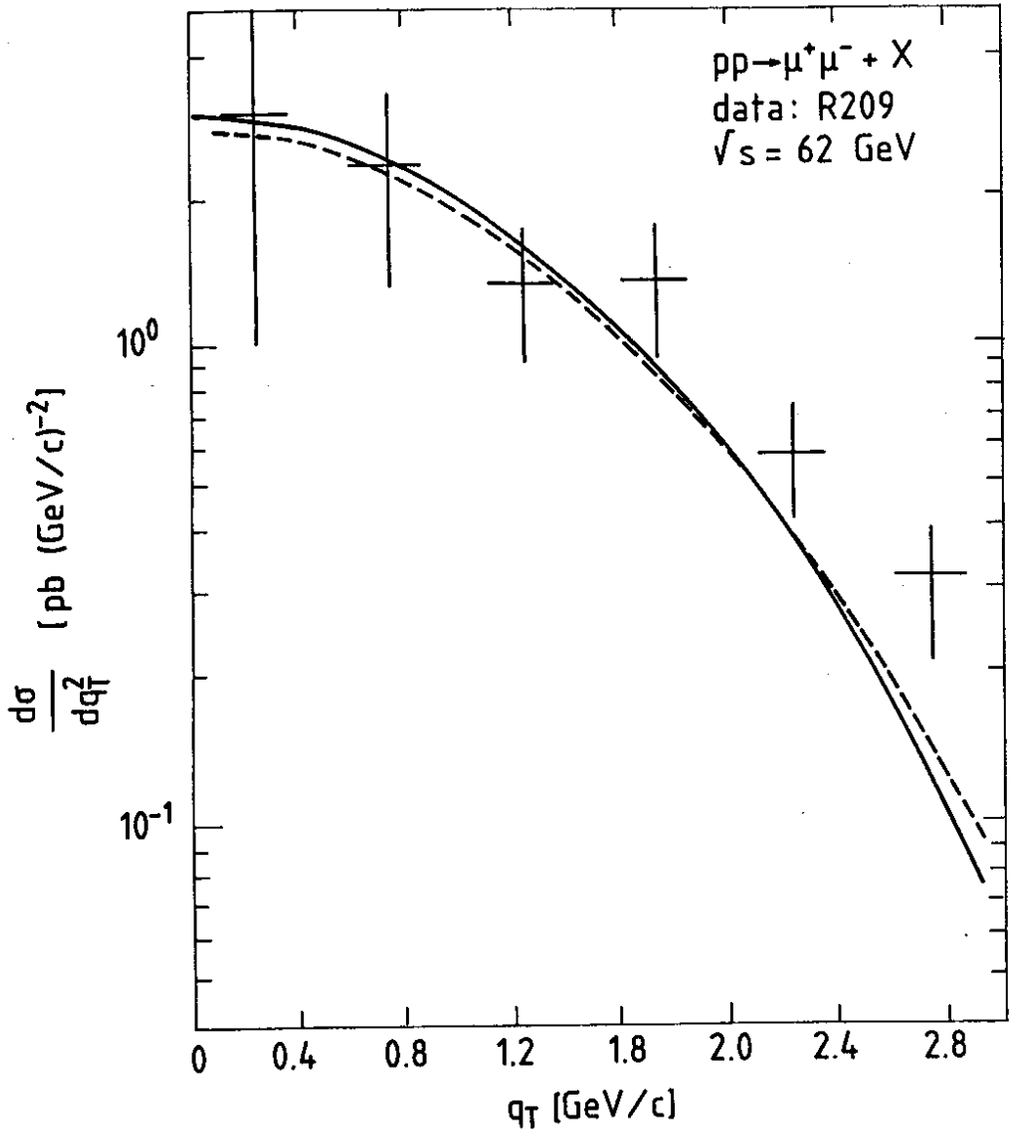
pp→μ⁺μ⁻ + X
data: R209
√s = 62 GeV
dσ/dq_T² [pb (GeV/c)⁻²]
10⁰
10⁻¹
0
0.4
0.8
1.2
1.8
2.0
2.4
2.8
q_T [GeV/c]

Fig. 5

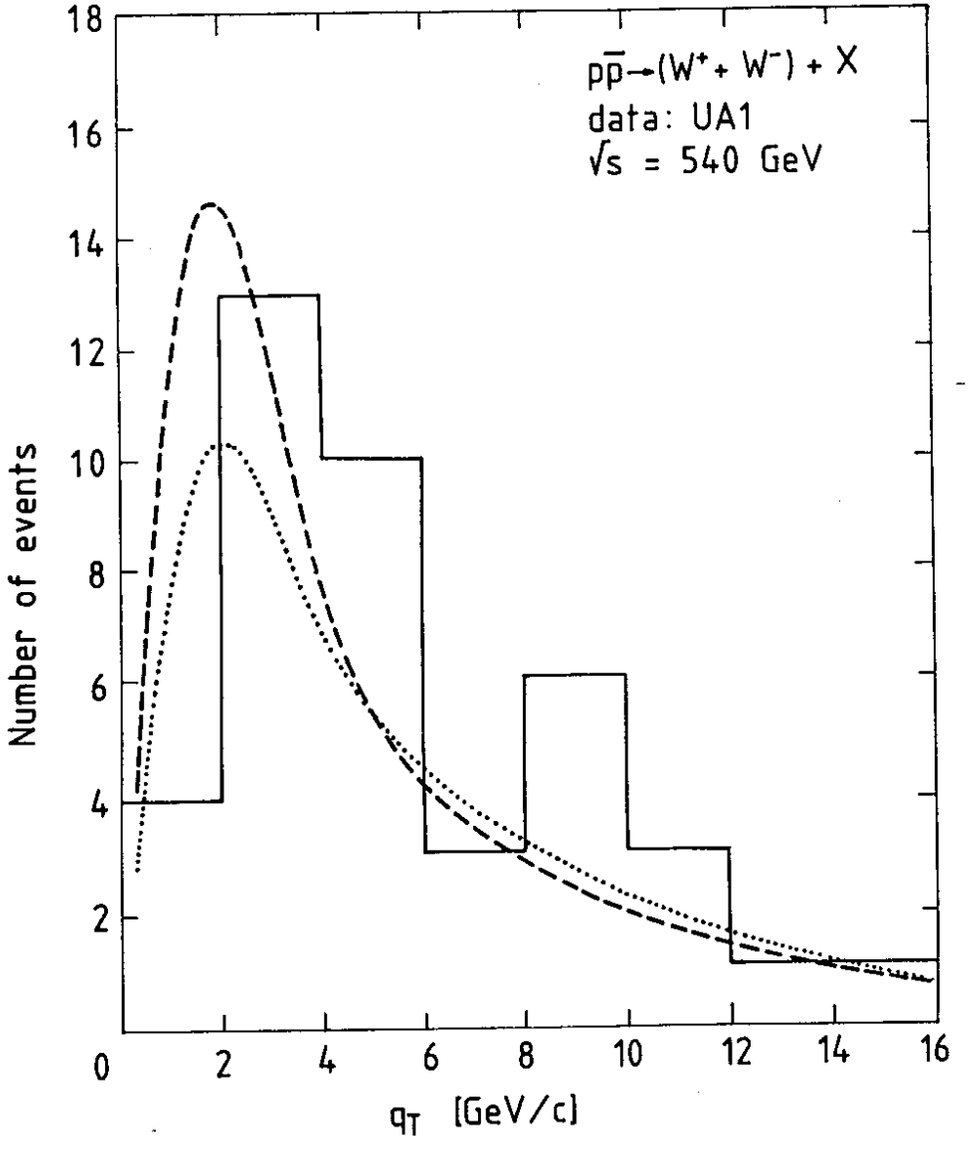
pp̄→(W⁺+ W⁻) + X
data: UA1
√s = 540 GeV
Number of events
18
16
14
12
10
8
6
4
2
0
2
4
6
8
10
12
14
16
q_T [GeV/c]

Fig. 6

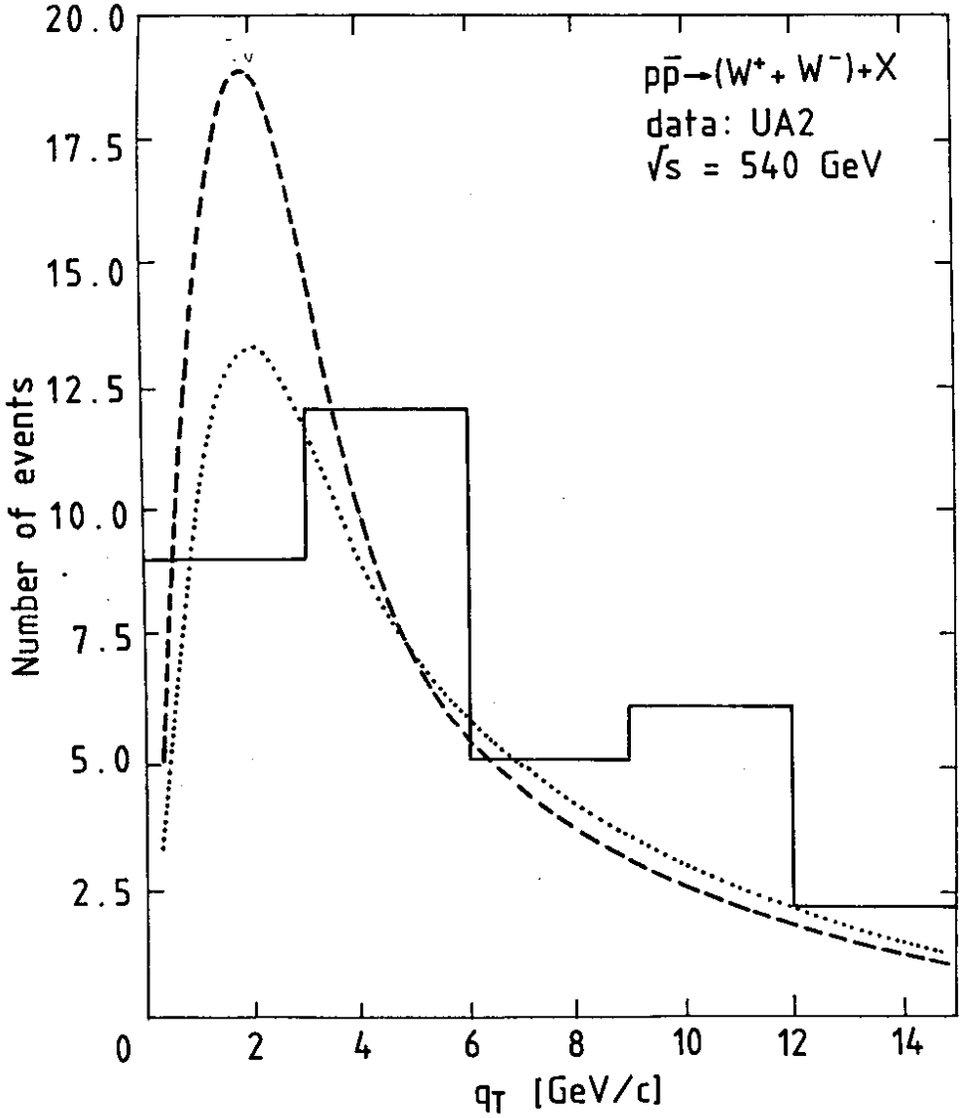
$p\bar{p} \rightarrow (W^+ + W^-) + X$
data: UA2
$\sqrt{s}$ = 540 GeV
Number of events
q_T [GeV/c]
20.0
17.5
15.0
12.5
10.0
7.5
5.0
2.5
0
2
4
6
8
10
12
14

Fig. 7

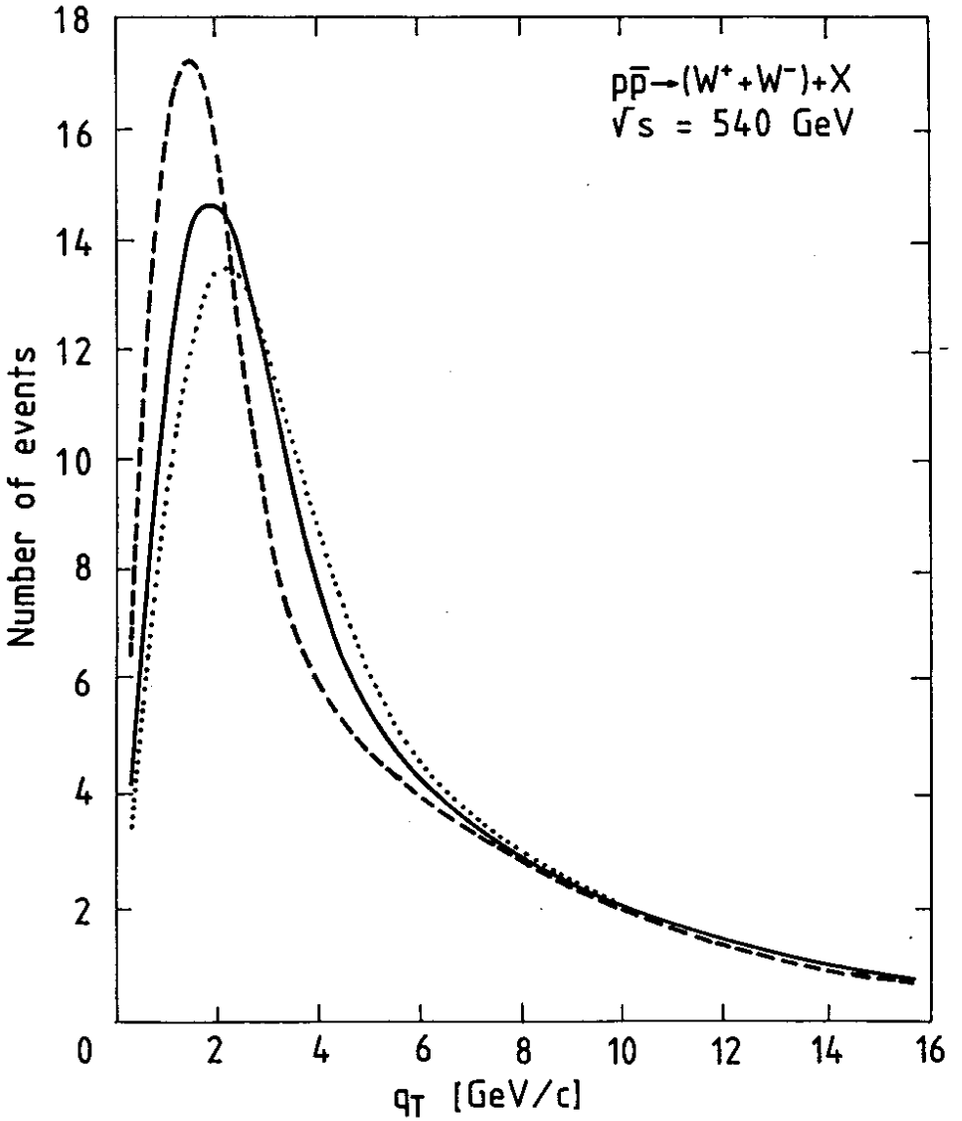
$p\bar{p} \rightarrow (W^+ + W^-) + X$
$\sqrt{s}$ = 540 GeV
Number of events
q_T [GeV/c]
18
16
14
12
10
8
6
4
2
0
2
4
6
8
10
12
14
16

Fig. 8

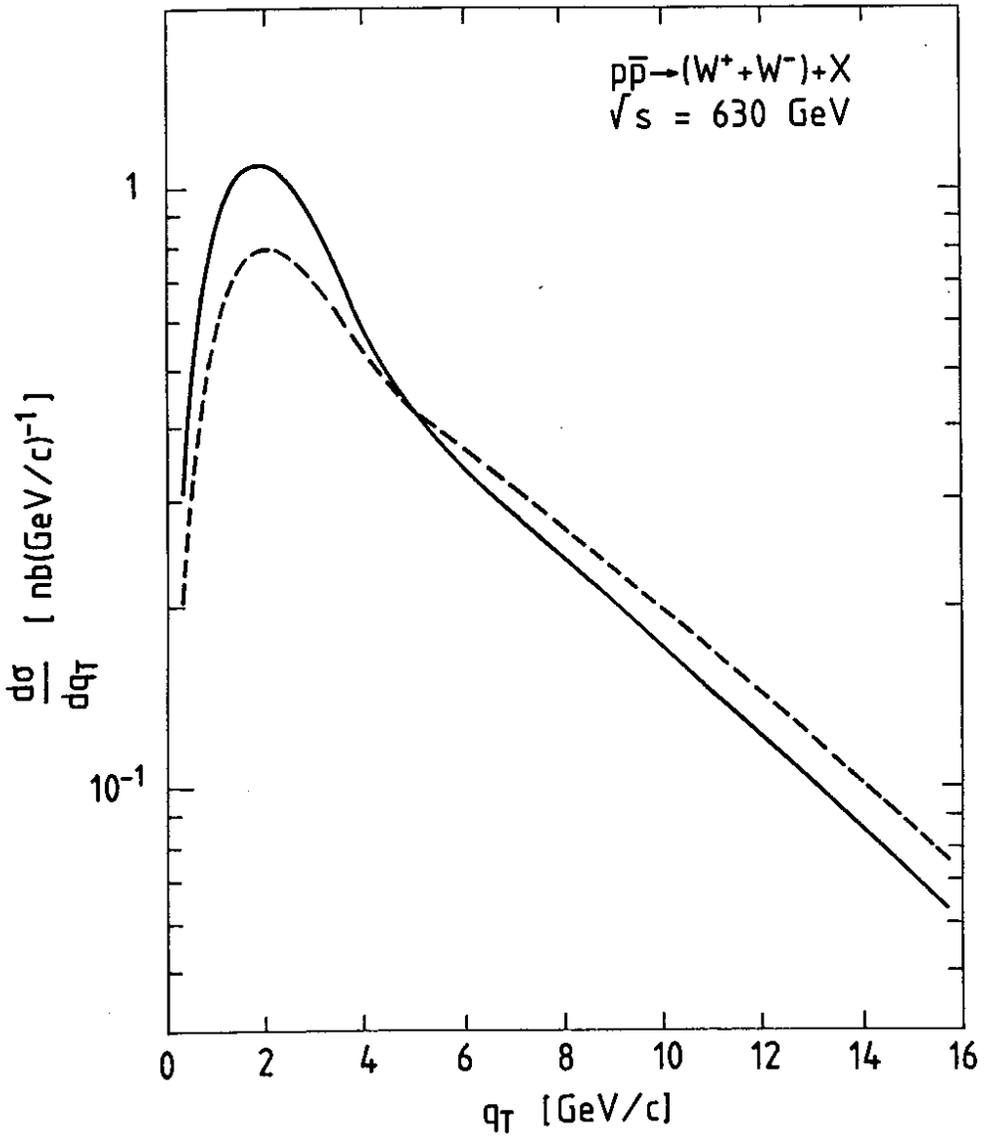
$p\bar{p} \to (W^+ + W^-) + X$
$\sqrt{s}$ = 630 GeV
$\frac{d\sigma}{dq_T}$ [nb(GeV/c)$^{-1}$]
1
10^{-1}
0
2
4
6
8
10
12
14
16
q_T [GeV/c]

Fig. 9

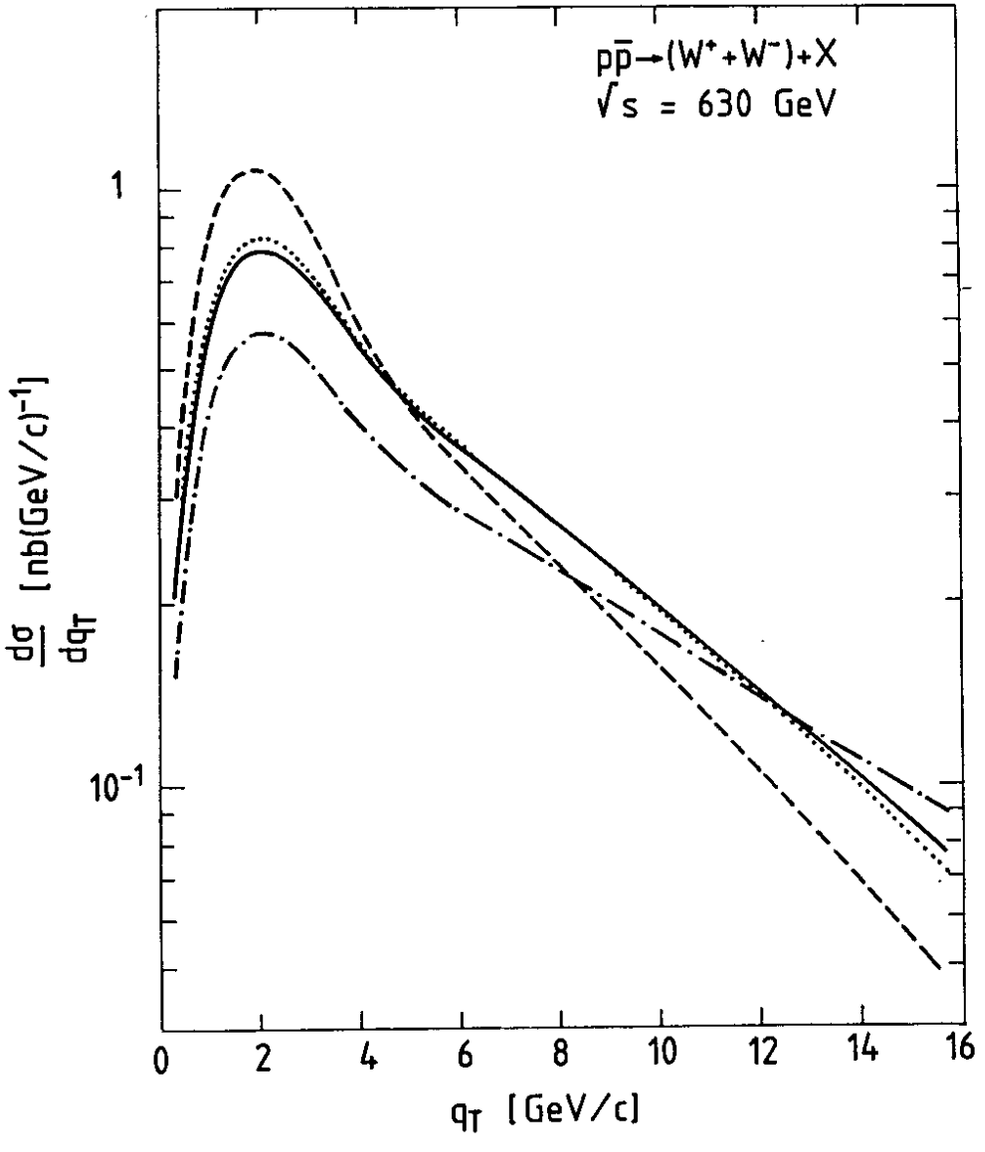
$p\bar{p} \to (W^+ + W^-) + X$
$\sqrt{s}$ = 630 GeV
$\frac{d\sigma}{dq_T}$ [nb(GeV/c)$^{-1}$]
1
10^{-1}
0
2
4
6
8
10
12
14
16
q_T [GeV/c]

Fig. 10

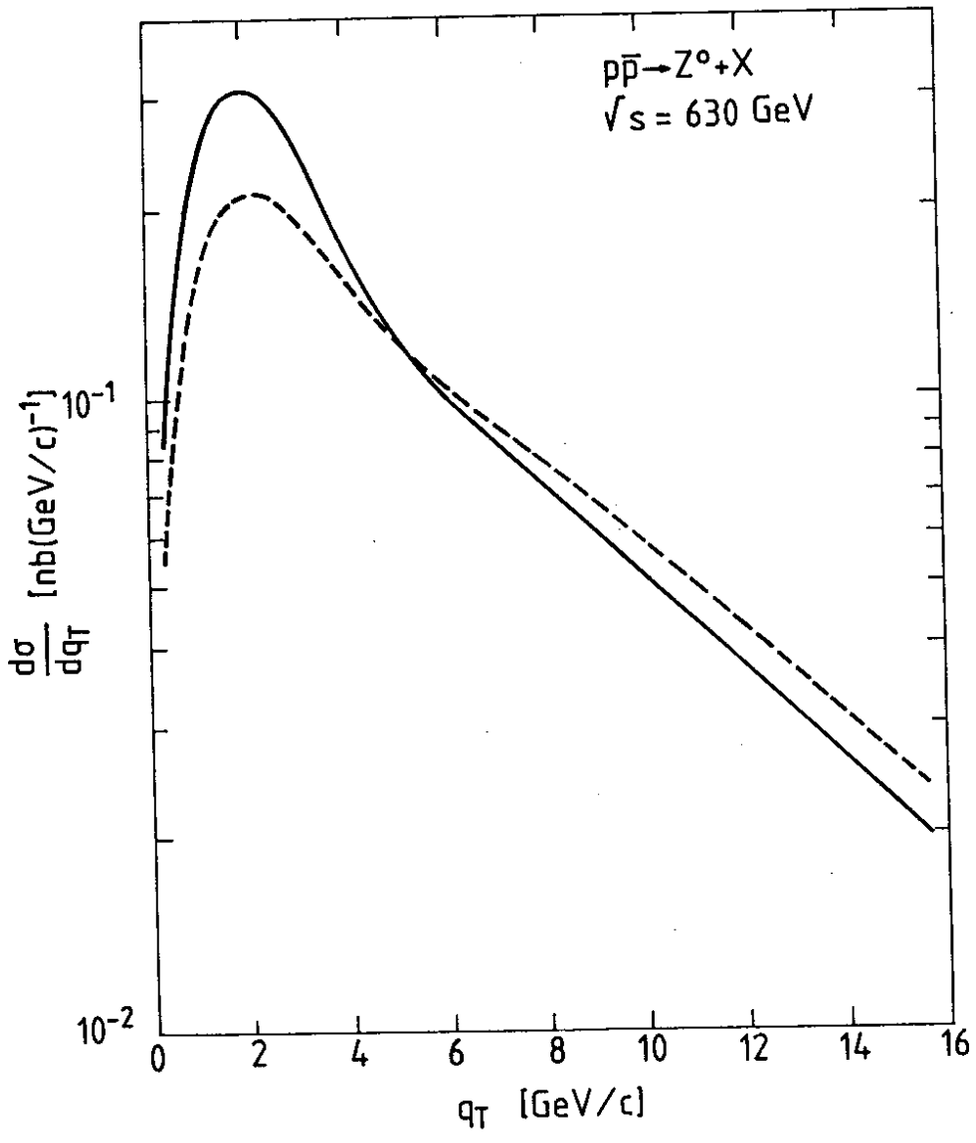
$p\bar{p} \to Z^0 + X$
$\sqrt{s}$ = 630 GeV
$\frac{d\sigma}{dq_T}$ [nb(GeV/c)$^{-1}$]
10^{-1}
10^{-2}
0
2
4
6
8
10
12
14
16
q_T [GeV/c]

Fig. 11

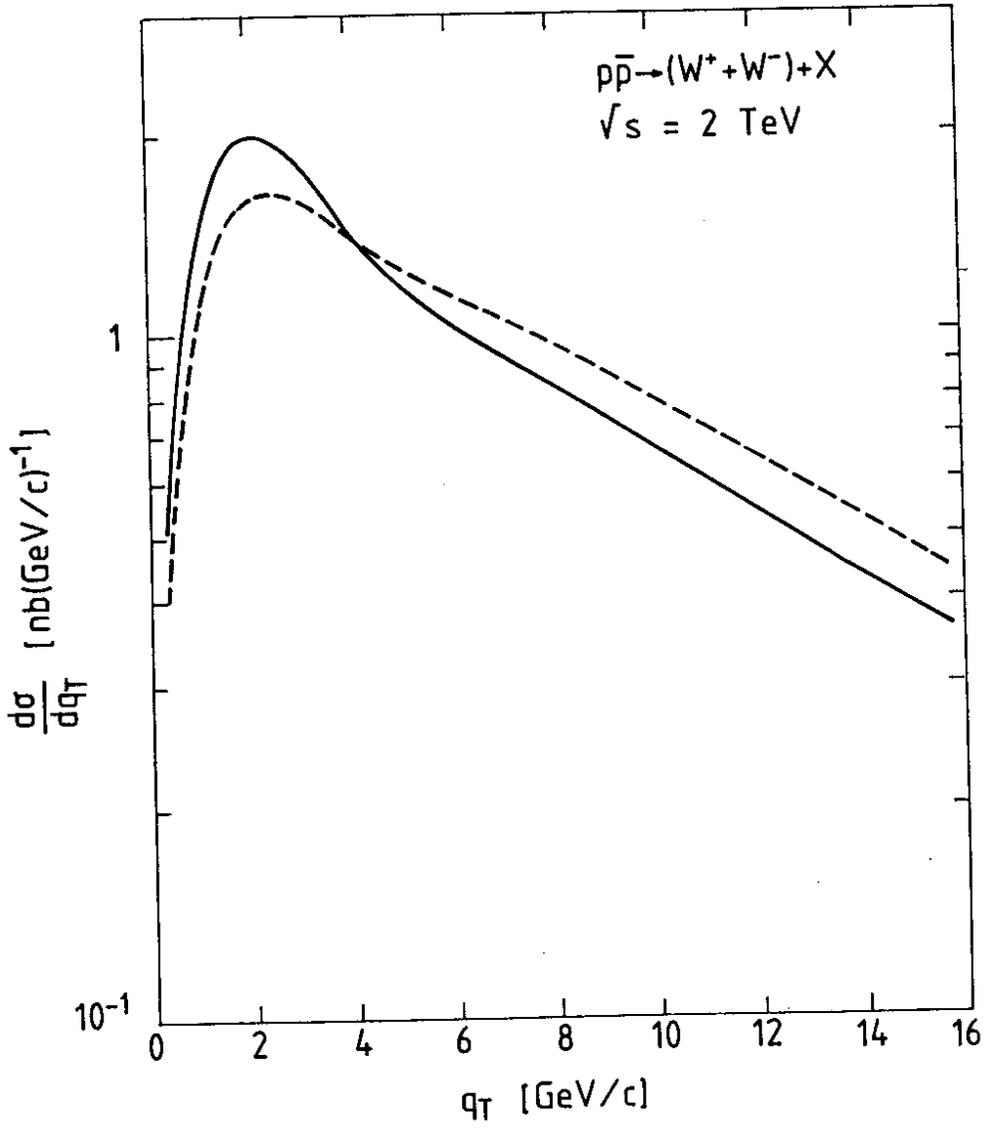
$p\bar{p} \to (W^+ + W^-) + X$
$\sqrt{s}$ = 2 TeV
$\frac{d\sigma}{dq_T}$ [nb(GeV/c)$^{-1}$]
1
10^{-1}
0
2
4
6
8
10
12
14
16
q_T [GeV/c]

Fig. 12

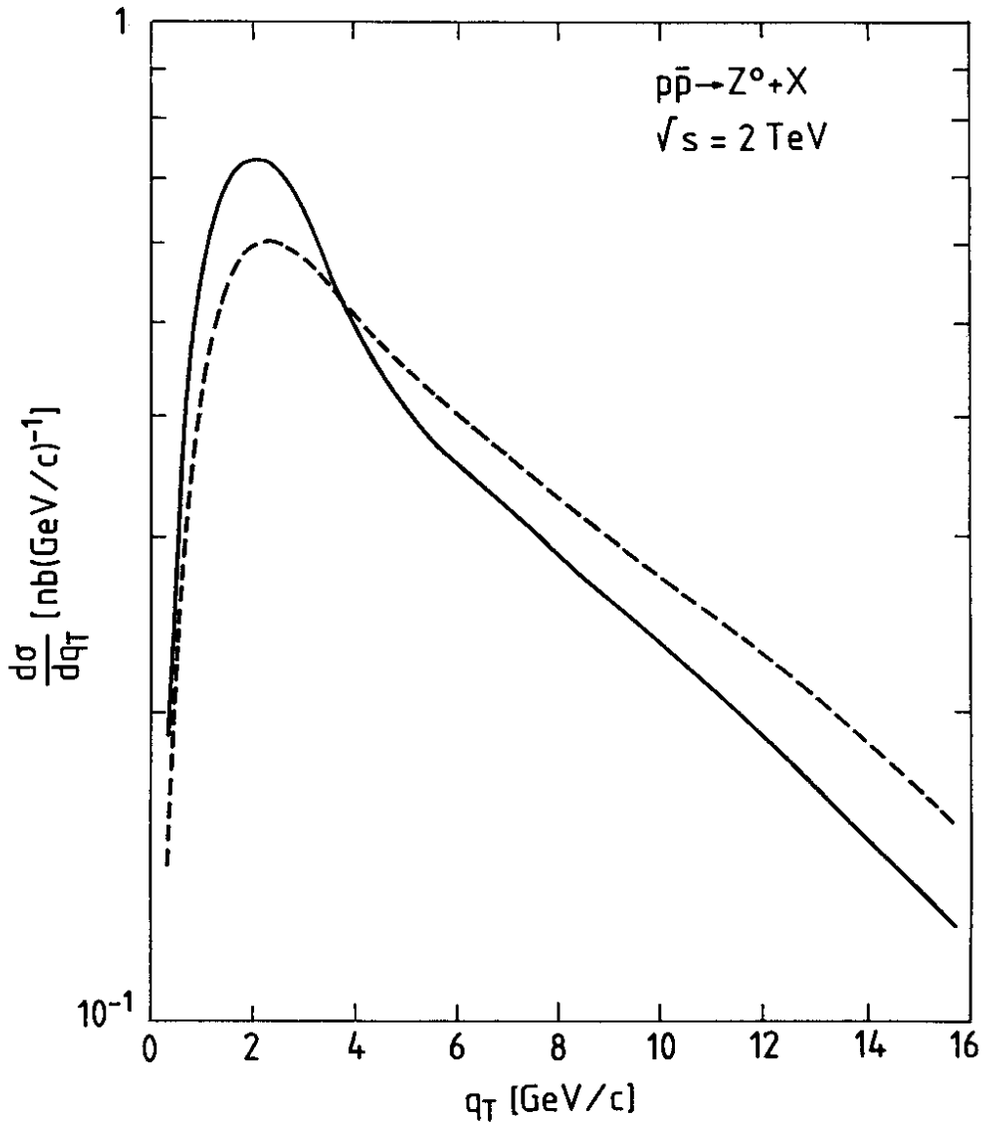
1
$p\bar{p} \rightarrow Z^0 + X$
$\sqrt{s} = 2$ TeV
$\frac{d\sigma}{dq_T}$ [nb(GeV/c)$^{-1}$]
10^{-1}
0
2
4
6
8
10
12
14
16
q_T [GeV/c]

Fig. 13